Joint Activity Detection and Channel Estimation for Clustered Massive Machine Type Communications

Leatile Marata, *Member, IEEE*, Onel Luis Alcaraz López, *Member, IEEE*, Andreas Hauptmann, *Senior Member, IEEE*, Hamza Djelouat, *Student Member, IEEE*, and Hirley Alves, *Member, IEEE*

Abstract

Compressed sensing multi-user detection (CS-MUD) algorithms play a key role in optimizing grant-free (GF) non-orthogonal multiple access (NOMA) for massive machine-type communications (mMTC). However, current CS-MUD algorithms cannot be efficiently parallelized, which results in computationally expensive implementations of joint activity detection and channel estimation (JADCE) as the number of deployed machine-type devices (MTDs) increases. To address this, the present work proposes novel JADCE algorithms that can be applied in parallel for different clusters of MTDs by exploiting the structure of the pilot sequences. These are the approximation error method (AEM)-alternating direction method of multipliers (ADMM) and AEM-sparse Bayesian learning (SBL). Results presented in terms of the normalized mean square error and the probability of miss detection evince comparable performance to the conventional algorithms. However, both AEM-ADMM and AEM-SBL algorithms have significantly reduced computational complexity and run-times, thus, increasing network scalability.

Index Terms

Leatile Marata, Onel Luis Alcaraz López, Hamza Djelouat, and Hirley Alves are with Centre for Wireless Communications – Radio Technologies, FI-90014, University of Oulu, Finland. e-mail: {leatile.marata,onel.alcarazlopez,hamza.djelouat, hirley.alves}@oulu.fi.
Andreas Hauptmann is with the Research Unit of Mathematical Sciences, FI-90014, University of Oulu, Finland, and also with the Department of Computer Science, University College London, London WC1E 6BT, U.K. e-mail: andreas.hauptmann@oulu.fi

This work is supported by Academy of Finland (Grants n.319485, n.340171, n.346208 (6G Flagship), n. 338408, n. 353093). The work of Leatile Marata was supported in part by the Riitta ja Jorma J. Takanen Foundation and the Botswana International University of Science and Technology. The work of Onel López was supported in part by the Finnish Foundation for Technology Promotion. The work of Hamza Djelouat was supported in part by the Tauno Tönning Foundation.

Approximation error method, detection, grant-free, machine-type communication, MIMO, sparse signal recovery.

I. Introduction

Detection, channel estimation, and data decoding are fundamental operations performed by a receiver in a wireless communication network [1]–[3]. However, the majority of algorithms designed for these operations in previous wireless communication systems, i.e., fourth-generation (4G) and earlier, were tailored exclusively for downlink human-type communications (HTC) [4], [5]. In a turn of events, the new communication standards, i.e., the fifth generation (5G) and beyond (5GB), natively support a new set of devices termed machine-type devices (MTDs), which perform various sensing tasks in the Internet of Things (IoT) paradigm [6]–[8]. Notably, MTDs are energy constrained, yet in some cases, they need to be deployed in remote areas where they cannot be readily charged. For this reason, MTDs are designed to save energy by only switching to active transmission mode after sensing data and remaining in sleep mode in the absence of data. This intermittent mode of operation reduces energy consumption while creating sporadic uplink traffic, which is unconventional to HTC. Since the modus operandi of the MTDs is incompatible with existing HTC devices, a verbatim implementation of existing receive algorithms in massive machine-type communication (mMTC) networks can degrade communication performance. Fortunately, the aforementioned problems can be jointly addressed by employing low-complexity transmission schemes, for which grant-free (GF) non-orthogonal multiple access (NOMA) plays a pivotal role.

GF-NOMA techniques have been proposed as low complexity transmission schemes for uncoordinated transmissions of the MTDs [9], [10]. Under these schemes, active devices transmit their data without the permission from the base station (BS), thus bypassing the signaling overheads that are associated with the handshaking/scheduling process and consequently reducing communication overheads and access latency [9], [10]. Nevertheless, the lack of scheduling and the inevitable use of non-orthogonal pilot sequences lead to both increased collisions and multi-user interference (MUI). Clearly, an inefficient use of GF-NOMA can be detrimental to the previously mentioned operations (detection, channel estimation, and data decoding), and this is one of the major drawbacks of GF-NOMA. Ultimately, the performance of GF-NOMA schemes relies on efficiently resolving both the collisions and MUI [11].

The need for efficient GF-NOMA has motivated compressed sensing (CS) multi-user detection (MUD) for joint activity detection and channel estimation (JADCE) and/or unsourced random access (URA) [12]. The former is concerned with both user identification and data decoding while the latter is mostly concerned with decoding the transmitted data as opposed to identifying the actual transmitting MTD [13]. As a result, JADCE is applicable in status update scenarios with different types of messages, e.g., when there are different MTDs for sensing ambient humidity, acidity, and temperature. Conversely, URA can be employed in scenarios where multiple MTDs transmit observations pertaining to a common physical phenomenon, such as temperature measurements in a smart factory, with the goal of obtaining average information of this phenomenon.

By and large, both JADCE and URA rely on the fact that a relatively small number of MTDs are simultaneously active in a given coherence interval (CI) despite their massive numbers. For instance, future networks are expected to host up to 10 million MTDs per km^2, while only a small fraction of them will be active at the same time. The identification of the active MTDs can naturally be posed as a CS-MUD problem, which can be computationally complex [14], [15]. However, with the increasing deployments of IoT, some of the MTDs are bound to present similar characteristics and performance requirements. These similarities can naturally facilitate the formation of clusters [16]–[19]. Basically, clusters of the MTDs can be formed according to the channel statistics (e.g., channel covariance matrix), performance requirements, traffic characteristics, or activation probabilities, among other things [19]. Given these considerations, clustering the MTDs can help optimize resource allocation, thus making the network design more flexible and scalable, which can lead to simplifying some CS-MUD problems. Consequently, a more practical optimization of GF-NOMA for a massive number of MTDs can be achieved by leveraging the clusters.

There is a noteworthy research endeavor to develop scalable algorithms for CS-MUD to optimize GF-NOMA. Typically, these methods utilize the massive multiple-input multiple-output (mMIMO) technology, which enables distributed or parallel signal processing. In a quest to accommodate a massive number of MTDs, most of the works rely on pilot data designed from fully non-orthogonal sequences [20]–[24]. Even though non-orthogonality of the pilot sequences is crucial for serving a massive number of MTDs, it is possible to create pilot sequences that can be grouped into finite orthogonal subspaces to capture/realize different clusters. Given the orthogonal subspaces, it is practical to implement CS-MUD algorithms in parallel while maintaining zero MUI across the clusters. Ultimately, this reduces the need for information exchange while the algorithms are running in parallel. Equally important is to note that such pilot sequences have to be formed using non-independent identically distributed (i.i.d.) sequences such as Hadamard, Zadoff Chu, and Fourier matrices, all of which are consistent with the 3GPP standard. As noted by Liu *et al.* [25], using i.i.d. pilot sequences is impractical, and most CS-MUD algorithms designed thus far to work under this assumption face challenges in practical scenarios. It is, therefore, crucial to devise practical approaches that facilitate the efficient implementation of CS-MUD algorithms while considering the existence of clusters in mMTC. To the best of our knowledge, there have not been any works on CS-MUD algorithms that consider the pilot subspaces of different clusters to be orthogonal to each other. To that end, the present work proposes novel CS-MUD solutions in the form of JADCE algorithms for clustered mMTC. Some of the advantages of the proposed algorithms are: i) reduced MUI, ii) efficient resource usage, iii) scalability, and iv) network design flexibility, all of which contribute to an efficient signal recovery. To provide context, we present a brief literature survey of related works.

A. Related Literature

In the recent past, mMIMO-enabled mMTC has become an active area of research. mMIMO is specifically crucial for mMTC due to its ability to increase spectral efficiency, data rates, and link reliability [26]. There are some ongoing works to develop efficient CS-MUD algorithms for GF-NOMA using mMIMO. For example, He *et al.* [27] proposed a distributed detection algorithm based on expectation propagation (EP) to facilitate integration at the central processing unit (CPU). The proposed work also presented a performance analysis of the EP in a distributed cell-free (CF)-MIMO. However, although the proposal improves the detection performance, it also increases the computational complexity of the CPU. On a similar note, Li *et al.* [28] proposed a covariance-based device activity detection algorithm that exploits orthogonal pilot sequences to reduce the MUI. Relative to existing works, their results showed improved performance for low signal-to-noise ratio (SNR) and short pilot lengths. On the other hand, Ganesan *et al.* [22] presented a maximum likelihood (ML) based device detection algorithm for CF-MIMO. Their results demonstrated improved performance when using CF-MIMO as opposed to co-located MIMO. In general, ML algorithms proposed in [22], [28] have high computational complexity. In a quest for lower-complexity algorithms, Bai *et al.* [29] proposed a distributed approximate message passing (AMP) algorithm based on the likelihood ratio fusion by exploiting the structure of the state evolution. However, it should be noted that AMP algorithms are only guaranteed to converge if the columns of the pilot matrix are drawn from a Gaussian distribution and columns are highly uncorrelated. Notably, [22], [26]–[29] all assume that devices are synchronized, which inspired Li *et al.* [30] to provide a different perspective and propose an asynchronous device activity detection in CF-MIMO systems where communication between the BSs and the CPU are optimized. From the results of [30], it is apparent that one of the bottlenecks of decentralized algorithms is the communication overhead incurred by increased signaling between the different sub-processors. In a similar vein, Chen *et al.* [31] proposed a structured massive access for CF-MIMO using the per group and the IB-K-means clustering algorithms. Their work showed an improved spectral efficiency of the proposed pilot assignment strategies, outperforming conventional pilot assignments. In addition, Figueredo *et al.* [32] presented a feasibility study for improving system capacity by clustering the MTDs such that they can share the same time-frequency resource blocks. Iimori *et al.* [33] proposed a bi-linear message passing algorithm that efficiently detects clusters of devices by leveraging the sparsity in the sub-arrays of extra-large MIMO.

Despite the potential benefit of capturing the clusters of MTDs using orthogonal pilot subspaces to facilitate efficient parallel implementation of JADCE algorithms, this has not been explored in the literature. Motivated by the work [34], where Marata *et al.* proposed some pilot design strategies to enable the amicable coexistence of different services, we present novel CS-MUD algorithms that exploit the pilot structure of the clusters of MTDs in mMTC scenarios.

B. Contributions

We consider an mMIMO network serving heterogeneous clusters of MTDs[1]. By capturing the heterogeneous characteristics of the MTDs using orthogonal pilot subspaces, we present a JADCE problem and solve it using parallel algorithms. Notice that, the present work departs from works such as [22], [26]–[29], where some iteration steps are exchanged even in parallel implementations of the CS-MUD algorithms. We summarize our main contributions as follows:

- We formulate the JADCE problem based on pilot subspaces, i.e., where the massive non-orthogonal pilot sequences of the MTDs of each cluster are computed from orthogonal subspaces. Some of the main advantages of the proposed formulation are the parallel

[1] Here, heterogeneity refers to differences in characteristics and performance requirements of the MTDs.

implementation of the sparse signal recovery (SSR) algorithms, network design flexibility, and scalability.

- We propose data-driven algorithms that utilize the approximation error method (AEM) established in the field of inverse problems to account for errors in the sensing matrix and likelihood function [35]–[37]. Herein, AEM is used to account for the mismatch between the ideal measurement and the measurement used to perform JADCE in each cluster. First, we propose the AEM-alternating direction method of multipliers (ADMM), which leverages the learned statistics of the mismatch to perform iterative soft thresholding. Second, we present the AEM-sparse Bayesian learning (SBL) algorithm which exploits a corrected likelihood function within the Bayesian framework. AEM-ADMM does not take the prior distribution into consideration and is applicable for scenarios without distributions of the parameters. On the other hand, AEM-SBL relies on statistical distributions, thus utilizing more information to improve the JADCE performance.
- We compare the proposed JADCE framework with the conventional approaches, which are applied without clustering, and numerically quantify their performance. Specifically, we show that our proposed algorithms achieve comparable channel estimation accuracy and detection capabilities to their classical counterparts while benefiting from reduced run-time.

C. Organization and Notation

The remainder of this paper is organized as follows. In Section II, we present and discuss the system model. In Section III, we introduce the cluster-based device activity detection problem. In Section IV, we propose the solutions to this problem, while Section V presents the results and discussions. Lastly, in Section VI, we conclude the paper and discuss some future research directions.

Notation: In the sequel, boldface lowercase, and boldface uppercase letters denote column vectors and matrices, respectively. Moreover, $\mathbf{a}_i$ and $a_{i,j}$ are the i-th column and the element in the i-row, j-th column of matrix $\mathbf{A}$, respectively, while a_i is the i-the element of vector $\mathbf{a}$. The superscripts $(\cdot)^*$, $(\cdot)^{\mathrm{T}}$, and $(\cdot)^{\mathrm{H}}$ denote the conjugate, transpose, and conjugate transpose operations, respectively. For both matrices and vectors, the hat notation indicates an estimate, e.g., $\hat{x}$ is the estimate of x. Additionally, $\mathbb{C}$ and $\mathbb{R}$ refer to complex and real domains, respectively. We denote the circularly symmetric complex Gaussian distribution with mean $\mathbf{a}$ and covariance $\mathbf{B}$ by $\mathcal{CN}(\mathbf{a}, \mathbf{B})$, while $\mathbb{E}\{\cdot\}$ and $\mathbb{V}\{\cdot\}$ are the expectation and covariance operators, respectively. The

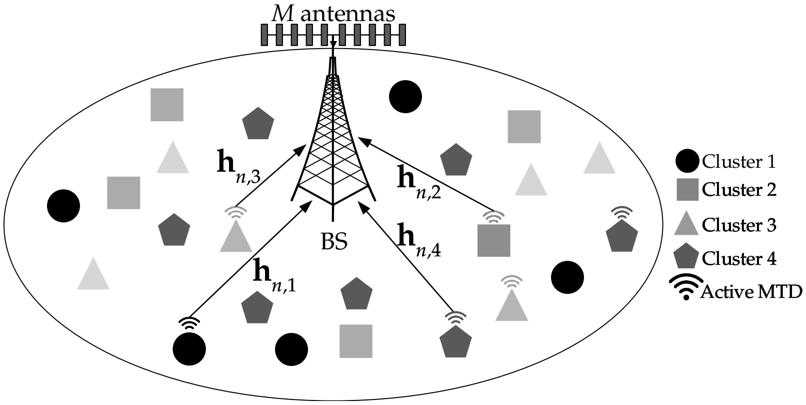

Fig. 1: An mMTC scenario where an M-antenna BS serves N MTDs grouped into G clusters, among which an average total of ϵN MTDs are active.

$\mathrm{diag}\{a_1, a_2, \cdots, a_n\}$ creates a diagonal matrix whose main diagonal terms are $a_1, a_2, \cdots, a_n$. Finally, $\|\cdot\|_F$ and $\|.\|_p$ denote the Frobenius and ℓ_p norms, respectively, while the probability distribution of random variables is defined as $\mathcal{P}(\cdot)$, while $\mathcal{P}(\cdot|\cdot)$ is the conditional probability.

II. System Model

We consider the uplink massive MIMO scenario depicted by Fig 1, where a BS equipped with a set of M antennas, i.e., $\mathcal{M} = \{1, \cdots, M\}$ serves a set $\mathcal{N} = \{1, \cdots, N\}$ of stationary MTDs. Among these, a subset $\mathcal{K} \subset \mathcal{N}$ of cardinality $K = |\mathcal{K}|$ is active and unknown to the BS. The MTDs are assumed to be active with a probability $\epsilon \ll 1$, thus the average number of active devices in the network in a given CI is ϵN. Moreover, $\mathcal{N}$ is sub grouped into a set of clusters sub-indexed by $\mathcal{G} = \{1, \cdots, G\}$, where $G \leq N$ and each MTD exclusively belongs to a cluster $\mathcal{C}_g \subseteq \mathcal{N}$, $g \in \mathcal{G}$. The cardinality of the g-th cluster is defined as N_g, such that $\sum_{g=1}^{G} N_g = N$.

We also assume quasi-static block fading channels where channels remain unchanged during each CI of T symbols and change independently from one CI to another one. We assume that only the large-scale channel state information (CSI), i.e., the path loss information, is available at the BS and not the instantaneous CSI. The uplink channel between the n-th MTD in the g-th cluster and the BS in a given CI is defined as $\mathbf{h}_{n,g} \sim \mathcal{CN}(\mathbf{0}, \beta_{n,g}\mathbf{I}) \in \mathbb{C}^{M \times 1}$, where $\{\beta_{n,g}\}$ are the path-losses. Let $\alpha_{n,g}$ denote the activation status of device n in the g-th cluster as

$$\alpha_{n,g} = \begin{cases} 1, & \text{if device } n \text{ in the } g\text{-th cluster is active} \\ 0, & \text{otherwise} \end{cases}, \tag{1}$$

hence, the overall network activity indicator is given by the vector $\boldsymbol{\alpha}=[\boldsymbol{\alpha}_1^{\mathrm{T}},\boldsymbol{\alpha}_2^{\mathrm{T}},\cdots,\boldsymbol{\alpha}_G^{\mathrm{T}}]^{\mathrm{T}} \in \{0,1\}^{N\times 1}$, where $\boldsymbol{\alpha}_g = [\alpha_{g,1},\alpha_{g,2},\cdots,\alpha_{g,N_g}]^{\mathrm{T}} \in \{0,1\}^{N_g\times 1}$, $\forall g$. The first phase of each CI (defined as the first L symbols) corresponds to the metadata processing block, i.e., where JADCE is carried out, while the other $T-L$ symbols are used to convey the intended message (payload). Each MTD is therefore pre-allocated a pilot sequence $\mathbf{s}_{n,g} \in \mathbb{C}^{L\times 1}$ that is known to both the BS and the MTD for JADCE[2]. However, due to the massiveness of the MTDs, the length of each pilot sequence is usually much smaller than the total number of devices, i.e., $L \ll N$. Consequently, the BS must pre-allocate non-orthogonal pilot sequences to all the MTDs and employ CS-MUD to solve the JADCE problem based on the signal received during the training phase which is given by,

$$\begin{aligned}\mathbf{Y} &= \sum_{\forall n,g} \alpha_{n,g}\mathbf{s}_{n,g}\mathbf{h}_{n,g}^{\mathrm{T}} + \mathbf{W}\\ &= \sum_{g=1}^{G} \mathbf{S}_g\mathbf{X}_g + \mathbf{W}\\ &= \mathbf{S}\mathbf{X}+\mathbf{W}, \end{aligned} \tag{2}$$

where $\mathbf{S}_g=[\mathbf{s}_{n,g},\cdots,\mathbf{s}_{N_g,g}]$, $\mathbf{X}_g=[\mathbf{x}_{1,g},\cdots,\mathbf{x}_{N_g,g}]^{\mathrm{T}}\ \forall g$, $\mathbf{S}=[\mathbf{S}_1^{\mathrm{T}},\cdots,\mathbf{S}_G^{\mathrm{T}}]^{\mathrm{T}}$, and $\mathbf{X}=[\mathbf{X}_1^{\mathrm{T}},\cdots,\mathbf{X}_G^{\mathrm{T}}]^{\mathrm{T}}$. Meanwhile, $\mathbf{W} \in \mathbb{C}^{L\times M}$ is the receiver noise, whose columns are i.i.d. as $\{\mathbf{w}\} \sim \mathcal{CN}(\mathbf{0},\sigma^2\mathbf{I}) \in \mathbb{C}^{L\times 1}$, while $\mathbf{x}_{n,g} = \sqrt{p_{n,g}}\alpha_{n,g}\mathbf{h}_{n,g} \in \mathbb{C}^{M\times 1}$ and $p_{n,g}$ are the effective row-sparse channel vector and the transmit power of the n-th device in the g-th cluster, respectively.

From (2), it is evident that if $\{\mathbf{S}_g\}$, $\forall g$, are created from orthogonal subspaces, it is possible to completely decentralize the JADCE process by performing the detection of each cluster separately, thus reducing the complexity of the problem. To this end, we subsequently discuss the formation of $\mathbf{S}_g$, $g=1,\cdots,G$, using orthogonal subspaces, which allows fully decentralized detection and channel estimation.

III. Decentralized detection as a CS problem

To achieve decentralization, we assume that the pilot sequences $\{\mathbf{S}_g \in \mathbb{C}^{L\times N_g}\}$ associated with each cluster are strictly generated as linear combinations of orthogonal basis matrices $\{\mathbf{B}_g \in \mathbb{C}^{L\times \kappa_g}\}$, such that $\sum_{\forall g}\kappa_g \leq L$. Let each $\mathbf{B}_g$,$\forall g$, be drawn from an orthogonal matrix

[2] Given that the pilot sequences are known *a priori* by the BS, it is possible to optimize their structure to improve the receive algorithms. To that end, we also present a combinatorial problem in Section III that can be solved at the BS to improve the detection capabilities.

defined as $\mathbf{B}=[\mathbf{B}_1,\mathbf{B}_2,\cdots,\mathbf{B}_G]\in\mathbb{C}^{L\times L}$, $\left\|\mathbf{B}_i^{\mathrm{H}}\mathbf{B}_j\right\|_F=0$, $\forall i\neq j$. As discussed in Section I, the number of MTDs is generally massive, and thus $N_g\geq L$ is a valid assumption. It is therefore computationally prohibitive to generate large $\mathbf{B}_g$. Furthermore, the CI is always finite, thus, infeasible to allocate mutually orthogonal pilot sequences to the MTDs belonging to the same cluster. Owing to the condition $N_g\geq L$, it is necessary to generate each $\mathbf{S}_g$ while guaranteeing signal recovery for each cluster, which is a fundamental problem in sensing (measurement) matrix design [38]. From CS perspectives, the matrix $\mathbf{S}_g$ guarantees signal recovery if it satisfies the restricted isometric property (RIP), formally stated as

$$(1-\delta_\epsilon)\left\|\mathbf{X}_g\right\|_F^2\leq\left\|\mathbf{S}_g\mathbf{X}_g\right\|_F^2\leq(1+\delta_\epsilon)\left\|\mathbf{X}_g\right\|_F^2,\forall\mathbf{X}_g,\tag{3}$$

such that $\left\|\mathbf{X}_g\right\|_{2,0}\leq K_g$, where K_g is the average number of active devices in a given cluster and $\delta_\epsilon>0$ is the restricted isometric constant [39].

Remark 1: The RIP can be interpreted as the ability of the matrix $\mathbf{S}_g$ to map $\mathbf{X}_g$ into the measurement space while maintaining the separation between the different samples of $\mathbf{X}_g$. This makes it possible to recover different samples of $\mathbf{X}_g$ without ambiguity.

From the Remark 1 and without any loss of generality, note that creating pilot sequences for two different MTDs within a cluster, i.e., $\mathbf{s}_{i,g}$ and $\mathbf{s}_{j,g}$, with $i\neq j$, involves maximizing the minimum distance between two distinct pilot sequences, i.e.,

$$\begin{aligned}&\underset{\mathbf{S}_g}{\text{maximize}}\quad\min_{1\leq i<j\leq|\mathcal{C}_g|}d(\mathbf{B}_g\mathbf{z}_i,\mathbf{B}_g\mathbf{z}_j)\\&\text{subject to}\quad\left\|\mathbf{z}_i\right\|_0=\left\|\mathbf{z}_j\right\|_0,\end{aligned}\tag{4}$$

where $d(\cdot,\cdot)$ is a generic distance measure between the two entries, while $\mathbf{z}_k\in\mathbb{C}^{K_g\times1}$, $k\in\mathcal{C}_g$ is a vector containing the random combining weights with an optimized cardinality. Observe that $\mathbf{z}_k$ must be sparse to guarantee good detectability, thus $\mathbf{s}_{k,g}=\mathbf{B}_g\mathbf{z}_k$, $k\in\mathcal{C}_g$, whereas the equality constraint in (4) ensures fairness.

Due to its combinatorial nature, the problem in (4) is NP-hard. To provide its approximate solution, we exploit the procedure discussed in Section IV-B of [34]. This will yield $\{\mathbf{S}_g\in\mathbb{C}^{L\times N_g}\}$ for each cluster, resulting in a concatenated pilot matrix $\mathbf{S}=[\mathbf{S}_1,\mathbf{S}_2,\cdots,\mathbf{S}_G]\in\mathbb{C}^{L\times N}$ of all the devices in the network[3]. This essentially leads to pilot sequences that are orthogonal to one another for different clusters, i.e., $|\mathbf{S}_i^{\mathrm{H}}\mathbf{S}_j|_F=0$, $\forall i\neq j$. Note that the resulting matrices $\{\mathbf{S}_g\}$ can have highly correlated columns, which can restrict the applicability of certain state-of-the-art

[3] To simplify the presentation, the matrix concatenation is assumed to follow the order of $g=1,\cdots,G$.

CS-MUD algorithms that rely on the AMP framework [10], [40].

A. Device Activity Detection as a CS problem

From definition (1) and the fact that traffic from MTDs is normally sporadic, the recovery of $\mathbf{X}$ constitutes a CS-MUD problem that can be solved using SSR concepts. Specifically, the BS has to identify the active devices from the compressed measurement $\mathbf{Y}$ with the knowledge that $\mathbf{X}$ is row-sparse. We can therefore define a generic inverse operation f of the form $\hat{\mathbf{X}}=f(\mathbf{Y},\mathbf{S})$, that maps the measurement into the effective channel space. Furthermore, due to the orthogonality of the subspaces, the inverse operation can further be cast as $\hat{\mathbf{X}}_g=f(\mathbf{Y}_g,\mathbf{S}_g)$ if $\mathbf{Y}_g$ is precisely known. Here, it is apparent that $\hat{\mathbf{X}}$ would be a solution from a centralized problem such as those in [10], [41], while $\hat{\mathbf{X}}_g$ would yield a solution for each cluster. Such an inverse operation can be formulated by exploiting Bayesian theory and/or a relaxed convex optimization framework.

For the Bayesian formulation, the sparsity promoting distribution of the effective channel $\mathbf{X}$ at each group level and within each group is modeled using the Bernoulli-Gaussian mixture distribution as [33]

$$\mathcal{P}(\mathbf{X})=\prod_{n,g}\Big((1-\epsilon)\delta(\mathbf{x}_{n,g})+\epsilon\mathcal{CN}(\mathbf{x}_{n,g};\mathbf{0},\beta_{n,g}\mathbf{I})\Big), \tag{5}$$

where $\delta(\cdot)$ is the dirac delta function imposing $\mathbf{x}_{n,g}=\mathbf{0}$ with a probability of $1-\epsilon$. From a mathematical perspective, precise knowledge of the linear problem (2) and (5) makes it possible to compute a Bayes optimal f to recover $\hat{\mathbf{X}}$ using the maximum a posterior (MAP) estimate. As a consequence, the optimal JADCE algorithm would choose a pair of $\boldsymbol{\alpha}$ and $\mathbf{X}$ using

$$\hat{\boldsymbol{\alpha}}=\underset{\boldsymbol{\alpha}}{\operatorname{argmax}}\int\mathcal{P}(\mathbf{X},\boldsymbol{\alpha}|\mathbf{Y})d\mathbf{X}, \tag{6}$$

$$\hat{\mathbf{X}}=\underset{\mathbf{X}}{\operatorname{argmax}}\int\mathcal{P}(\mathbf{X},\boldsymbol{\alpha}|\mathbf{Y})d\boldsymbol{\alpha} \tag{7}$$

from the joint posterior distribution

$$\mathcal{P}(\mathbf{X},\boldsymbol{\alpha}|\mathbf{Y})\propto\mathcal{P}(\mathbf{Y}|\mathbf{X},\boldsymbol{\alpha})\mathcal{P}(\mathbf{X}|\boldsymbol{\alpha})\mathcal{P}(\boldsymbol{\alpha}). \tag{8}$$

However, the optimal detector that computes (6) and (7) is not practically implementable in a receiver. Firstly, there is a lack of precise information about the activation probabilities of the MTDs and that makes it difficult to formulate the prior distribution $\mathcal{P}(\mathbf{X})$ accurately. Secondly, even if the prior distribution can be accurately computed, the marginalization of (8) requires prohibitively high dimensional integrals/summations with respect to a large number of variables in mMTC scenarios. For this reason, most solutions to (6) and (7) are sought using alternative approaches.

A common approach that relaxes the complex marginalization is to approximate the joint posterior distribution using belief propagation [42]. Such an approach yields an efficient solution via the sum-product algorithm. Another approach involves the approximation of the posterior distribution using mean field techniques, under which the solution is found through variational message passing [43], [44]. Alternatively, the solution can be sought from the relaxed convex optimization formulation

$$\underset{\mathbf{X}}{\text{minimize}}\, \frac{1}{2} \left\| \mathbf{Y} - \mathbf{S}\mathbf{X} \right\|_F^2 + \lambda \left\| \mathbf{X} \right\|_{2,1}, \tag{9}$$

where $\lambda \in \mathbb{R}^+$ serves as a penalty term that trades off measurement fidelity and sparsity structure captured by the mixed $\ell_{2,1}$ norm. Nevertheless, observe that (9) can also be computationally burdensome for large-scale problems and its effectiveness depends on properly choosing the penalty term. This is evidently sub-optimal compared to its Bayesian-based counterparts. However, it can achieve reasonable results and there have been some research efforts directed towards executing its solution in parallel, e.g., [45], [46]. As alluded to earlier, such parallel implementations cannot reap the full benefits of the proposed pilot-based cluster model because they rely on the ability to decompose the objective function as opposed to the possible isolation of the clusters of the MTDs. In the end, their parallel implementations require the exchange of the updates of the Lagrange multipliers. We subsequently present the AEM-inspired SSR solutions that perform JADCE while considering the existence of clusters.

IV. Approximation error method inspired Sparse Recovery

Considering that the problem (2) is formulated exploiting the fact that the pilot sequences $\mathbf{S}_i$ and $\mathbf{S}_j$ of $\mathcal{C}_i$ and $\mathcal{C}_j$, $i \neq j$, respectively, are orthogonal to each other, then the JADCE is broken down into smaller problems, one for each cluster. For example, the signal processing at the g-th cluster can depart from

$$\tilde{\mathbf{X}}_g = \mathbf{S}_g^{\mathrm{H}} \mathbf{Y}. \tag{10}$$

Interestingly, if the devices follow URA or have correlated activity, their joint activity can be estimated using $\|\tilde{\mathbf{X}}_g\|_F \geq \zeta$, where ζ should be greater but relatively close to $\frac{1}{\sqrt{L}}\sigma$ for good performance. The ability to handle both URA and correlated activity provides the much needed flexibility in pilot sequence allocation. For example, there is a flexibility to allocate larger basis

Algorithm 1: CB-SOMP, $\forall g \in \mathcal{G}$

```
Input: $\mathbf{Y}$, $\Delta$
$\hat{\mathbf{X}}_g^{(0)} = \mathbf{0}$
$\mathbf{R}_g^{(0)} = \mathbf{Y}$, $t = 0$, $\mathcal{H}_g^{(0)} = \emptyset$
repeat
    $\mathbf{D}^{(t)} = \mathbf{S}_g^{\mathrm{H}} \mathbf{R}_g^{(t)}$
    $j^{(t)} = \text{argmax}_j \left\{ \frac{\left\| \mathbf{d}_j^{(t)} \right\|_1}{\left\| \mathbf{s}_j \right\|_2} \right\}$
    $\mathcal{H}^{(t)} = \mathcal{H}^{(t)} \cup j^{(t)}$
    $\mathbf{X}_{[\mathcal{H}^{(t)}]}^{(t)} = \mathbf{S}_{[\mathcal{H}^{(t)}]}^{\dagger} \mathbf{Y}$
    $\mathbf{R}^{(t)} = \mathbf{Y} - \mathbf{S}\mathbf{X}^{(t)}$
    $t = t + 1$
until $\frac{\left\| \mathbf{X}^{(t)} - \mathbf{X}^{(t-1)} \right\|_F}{\left\| \mathbf{X}^{(t)} \right\|_F} < \Delta$;
Output: $\hat{\mathbf{X}}_{\mathbf{g}} = \mathbf{X}^{(t)}$
```

matrices $\mathbf{B}_g$ to devices that require more resources, such as those used in URLLC systems, as discussed by Lopez *et al.* in [19].

Observe that the decorrelation step (10) isolates the different clusters. However, $\tilde{\mathbf{X}}_g$ resulted from a backward projection of the measurement into the solution space, thus, relying on this statistic for the JADCE can lead to sub-optimal performance. This is because the majority of existing algorithms are specifically designed to utilize the low-dimensional measurements captured by $\mathbf{Y}$ in order to compute $\hat{\mathbf{X}}$. Evidently, $\tilde{\mathbf{X}}_g$ leads to the loss of crucial structures in the signal that is used for the JADCE at each cluster.

Remark 2: Observe from (10) that most CS-MUD algorithms that have the correlation step $\mathbf{S}_j^{\mathrm{H}}\mathbf{Y}$, $j \in \mathcal{G}$ among their iterative steps can provide a naive solution of the cluster based JADCE.

Following the Remark 2, we exemplify the implementation of the naive solution via simultaneous orthogonal matching pursuit (SOMP) [47]. In order to differentiate it from the traditional implementation of SOMP, we refer to the cluster-based implementation as cluster-based SOMP (CB-SOMP), which is outlined in **Algorithm** 1. In all the algorithms, Δ is the error tolerance level used in the stopping criteria.

As previously mentioned, the backward projection can be detrimental to the receiver's performance. A classical solution to map $\tilde{\mathbf{X}}_g$ back into the measurement space of each of the clusters is by using

$$\hat{\mathbf{Y}}_{\mathbf{g}} = (\mathbf{S}_g\mathbf{S}_g^{\mathrm{H}})^{-1}\mathbf{S}_g\tilde{\mathbf{X}}_g. \tag{11}$$

Meanwhile, similar to (8), the resulting reduced MAP problem has the joint posterior distribution

$$\mathcal{P}(\mathbf{X}_g, \boldsymbol{\alpha}_g|\hat{\mathbf{Y}}_g) \propto \mathcal{P}(\hat{\mathbf{Y}}_g|\mathbf{X}_g, \boldsymbol{\alpha}_g)\mathcal{P}(\mathbf{X}_g|\boldsymbol{\alpha}_g)\mathcal{P}(\boldsymbol{\alpha}_g). \tag{12}$$

It is important to note that the resulting MAP problem has lower dimensions than the one handled without clusters. In spite of this, a major drawback comes from the fact that the matrix $\mathbf{S}_g$ from (4) is of very low rank, and thus its pseudo-inverse results in a mismatched measurement, i.e.,$\hat{\mathbf{Y}}_g \neq \mathbf{Y}_g$, even under noise free conditions. Motivated by the AEM method from inverse problems and Bayesian AEM in [36], we account for this mismatch by imposing data-driven model corrections. The following subsection provides a brief background of the AEM-inspired solutions.

A. Review of AEM

This subsection briefly introduces the AEM [36], [37], [48], which is used to develop the proposed JADCE algorithms. AEM is utilized to address the numerical error between $\hat{\mathbf{Y}}_g$ and $\mathbf{Y}_g$ resulting from the pseudo-inverse operation (11), particularly when $\mathbf{S}_g$ is low-rank, as considered in the sequel. For this reason, $\hat{\mathbf{Y}}_g$ is not a reliable measurement of the received signal corresponding to the g-th cluster. However, the aim of JADCE is to recover/estimate a hidden variable $\mathbf{X}_g$ using some set of measurements while relying on their ideal linear relationship. This linear relationship is defined by a measurement matrix $\mathbf{S}_g$, which is assumed to be well known in advance and contains all the necessary information about how $\mathbf{X}_g$ is mapped into $\mathbf{Y}_g$. Such a relationship is modelled in noiseless scenarios by

$$\mathbf{Y}_g = \mathbf{S}_g\mathbf{X}_g. \tag{13}$$

To that end, relying solely on $\hat{\mathbf{Y}}_g$ to recover the hidden variable $\mathbf{X}_g$ is tantamount to using an incorrect linear model, thus, equivalent to using an incorrect measurement matrix.

Let $\tilde{\mathbf{S}}_g$ be the unknown and incorrect measurement matrix, then the relationship that yields $\hat{\mathbf{Y}}_g$ can be modelled by

$$\hat{\mathbf{Y}}_g = \tilde{\mathbf{S}}_g\mathbf{X}_g, \tag{14}$$

and introduces a systematic model error

$$\Delta\mathbf{Y}_g = \mathbf{Y}_g - \hat{\mathbf{Y}}_g. \tag{15}$$

Failure to account for this error has a negative impact on the JADCE performance. Fortunately, this discrepancy can be corrected by leveraging AEM concepts from the field of inverse problems [36], [48]. This is achieved by solving for $\mathbf{X}_g$ using a corrected version of the measurement matrix $\tilde{\mathbf{S}}_g$, and thus providing a general framework for CS-MUD that can be applied in cases where the sensing matrix has errors [49]. Essentially, we can approximate $\mathbf{S}_g$ by $\mathbf{C}_g\tilde{\mathbf{S}}_g \approx \mathbf{S}_g$, where $\mathbf{C}_g$ represents the correction term associated with the model error (15) and that can be obtained through statistical training. Since the MTDs are considered to be stationary, it is possible to acquire each $\mathbf{C}_g$ offline. In addition, this training process does not contribute to the computational complexity of the JADCE solutions. Precisely, $\mathbf{C}_g$ is computed from the covariance matrix of the model error, i.e., $\boldsymbol{\Phi}_g$, as will be discussed at the beginning of Section IV-B. First, the model error can be acquired in each cluster and considering τ training samples using

$$\mathbf{E}_g(i) = \mathbf{S}_g\mathbf{X}_g(i) - \hat{\mathbf{Y}}_g(i), i = 1, \cdots, \tau. \tag{16}$$

Here, $\mathbf{E}_g(i) = [\mathbf{e}_1(i), \cdots, \mathbf{e}_M(i)]$, where, $\mathbf{e}_m(i) = \mathbf{S}_g\mathbf{x}_m(i) - \tilde{\mathbf{S}}_g\mathbf{x}_m(i)$, corresponds to the mismatch error at the m-th antenna for the i-th training sample. By sufficiently training with (16), the average mismatch error for the m-th antenna is given by $\boldsymbol{\mu}_m = \sum_{i=1}^{\tau} \mathbf{e}_m(i)/\tau$. It then follows that the sample error covariance matrix of the mismatch error at the m-th antenna in a cluster is given by

$$\boldsymbol{\Omega}_m = \frac{1}{\tau - 1}\sum_{i=1}^{\tau} \mathbf{e}_m(i)\mathbf{e}_m(i)^{\mathrm{H}} - \boldsymbol{\mu}_m\boldsymbol{\mu}_m^{\mathrm{H}}, \tag{17}$$

which converges to the population covariance matrix as $\tau \to \infty$.

Remark 3: Given that the MTDs are stationary and by relying on the law of large numbers, the training at a single antenna is sufficient to provide the average covariance of the mismatch error for the g-th cluster, thus, $\boldsymbol{\Phi}_g = \mathbb{E}\{\boldsymbol{\Omega}_m\}$. Furthermore, with sufficient antenna spacing, $\boldsymbol{\Phi}_g$ is a diagonal matrix, and using it for AEM does not add to the computational complexity of the proposed algorithms.

Following this remark, we next introduce $\mathbf{C}_g$ into the optimization problem (9) and subsequently present the AEM-inspired JADCE solutions that are data-driven for each cluster.

B. Solution via AEM-ADMM

The first AEM-inspired solution is derived via the ADMM framework that relies on the iterative soft threshold algorithm (ISTA). From the discussion of the AEM, we note that the noisy measurement for each cluster is related to the results of its pseudo-inverse by

$$\begin{aligned}\mathbf{Y}_g &= \mathbf{S}_g\mathbf{X}_g + \mathbf{E}_g + \mathbf{W}\\ &= \hat{\mathbf{Y}}_g + \mathbf{E}_g\ ,\forall g,\end{aligned} \tag{18}$$

where $\mathbf{E}_g$ is the model error from (16) and $\mathbf{W}$ comes from (2). Given this, the net error from noise and the model error is defined as $\boldsymbol{\Xi}_g = [\boldsymbol{\xi}_1, \cdots, \boldsymbol{\xi}_M]$, such that $\boldsymbol{\Xi}_g = \mathbf{E}_g + \mathbf{W}$. By relying on the law of large numbers, we approximate each column of $\boldsymbol{\Xi}_g$ by a Gaussian variable, i.e., $\boldsymbol{\xi}_m = \mathbf{e}_1 + \mathbf{w}_i$, $\boldsymbol{\xi}_m \sim \mathcal{CN}(\boldsymbol{\psi}_m, \boldsymbol{\Omega}_m)$, where $\boldsymbol{\psi}_m$ is acquired through training, similar to $\boldsymbol{\mu}_m$. Given its Gaussian nature, $\boldsymbol{\xi}_m$ has a precision matrix with the Cholesky decomposition $\mathbf{C}_g^{\mathrm{T}}\mathbf{C}_g = \boldsymbol{\Phi}_g^{-1}$ and thus facilitates the formulation of the exponential likelihood function [36]

$$\mathcal{P}(\mathbf{Y}_g|\mathbf{X}_g) \propto \exp\left(-\frac{1}{2}\left\|\mathbf{C}_g\left(\mathbf{S}_g\mathbf{X}_g - \hat{\mathbf{Y}}_g + \boldsymbol{\Psi}_g\right)\right\|_F^2\right), \tag{19}$$

where $\boldsymbol{\Psi}_g = [\boldsymbol{\psi}_1, \cdots, \boldsymbol{\psi}_M]$. Therefore, the JADCE solution is

$$\begin{aligned}\hat{\mathbf{X}}_g &= \underset{\mathbf{X}_g}{\operatorname{argmax}}\, \mathcal{P}(\mathbf{Y}_g|\mathbf{X}_g)\mathcal{P}(\mathbf{X}_g)\\ &\overset{(a)}{=} \underset{\mathbf{X}_g}{\operatorname{argmax}}\, \ln\mathcal{P}(\mathbf{Y}_g|\mathbf{X}_g) + \ln\mathcal{P}(\mathbf{X}_g)\\ &\overset{(b)}{=} \underset{\mathbf{X}_g}{\operatorname{argmin}}\, \frac{1}{2}\left\|\mathbf{C}_g\left(\mathbf{S}_g\mathbf{X}_g - \hat{\mathbf{Y}}_g + \boldsymbol{\Psi}_g\right)\right\|_F^2 + \lambda\left\|\mathbf{X}_g\right\|_{2,1},\end{aligned} \tag{20}$$

where (a) comes from using the logarithmic form, while (b) leverages (19) while taking $\lambda\|\mathbf{X}_g\|_{2,1}$ as an approximation of $-\ln\mathcal{P}(\mathbf{X}_g)$. Notice that λ trades off between the measurement fidelity and the sparsity of the solution. To implement (20) via the ADMM framework [45], [46], we reformulate the problem (20) for each cluster $g \in \mathcal{G}$ as follows

$$\underset{\mathbf{X}_g,\mathbf{Z}_g}{\text{minimize}}\quad \frac{1}{2}\left\|\mathbf{C}_g\left(\mathbf{S}_g\mathbf{Z}_g - \hat{\mathbf{Y}}_g + \boldsymbol{\Psi}_g\ \right)\right\|_F^2 + \lambda\left\|\mathbf{X}_g\right\|_{2,1} + \frac{\rho}{2}\left\|\mathbf{X}_g - \mathbf{Z}_g\right\|_F^2 \tag{21a}$$

$$\text{subject to}\quad \mathbf{X}_g = \mathbf{Z}_g, \tag{21b}$$

where ρ is the ADMM step size and $\mathbf{Z}_g = [\mathbf{z}_{n,g}, \cdots, \mathbf{z}_{N_g,g}]^{\mathrm{T}}$ is the auxiliary variable that facilitates the closed form update of the estimate of $\mathbf{X}_g$ through the Moreau-Yosida regularization

[45]. Following the formulation (21), the augmented Lagrangian is expressed as [45]

$$\begin{aligned}\mathcal{L}\left(\mathbf{X}_g,\boldsymbol{\Theta}_g\right) &\overset{(a)}{=} \frac{1}{2}\left\|\mathbf{C}_g\left(\mathbf{S}_g\mathbf{Z}_g-\hat{\mathbf{Y}}_g+\boldsymbol{\Psi}_g\right)\right\|_F^2+\lambda\left\|\mathbf{X}_g\right\|_{2,1}+\boldsymbol{\Theta}_g^{\mathrm{T}}\left(\mathbf{X}_g-\mathbf{Z}_g\right)+\frac{\rho}{2}\left\|\mathbf{X}_g-\mathbf{Z}_g\right\|_F^2\\ &\overset{(b)}{=} \frac{1}{2}\left\|\mathbf{C}_g\left(\mathbf{S}_g\mathbf{Z}_g-\hat{\mathbf{Y}}_g+\boldsymbol{\Psi}_g\right)\right\|_F^2+\lambda\left\|\mathbf{X}_g\right\|_{2,1}+\left\|\mathbf{X}_g-\mathbf{Z}_g+\frac{\boldsymbol{\Theta}_g}{\rho}\right\|_F^2-\frac{\left\|\boldsymbol{\Theta}_g\right\|_F^2}{2\rho},\end{aligned} \tag{22}$$

where $\boldsymbol{\Theta}_g=[\boldsymbol{\theta}_{1,g},\cdots,\boldsymbol{\theta}_{N_g,g}]\in\mathbb{C}^{M\times N_g}$ is the dual matrix for the augmented Lagrangian. The expression of $\mathcal{L}\left(\mathbf{X}_g,\boldsymbol{\Theta}_g\right)$ in (a) is the standard augmented Lagrangian function, while (b) is the scaled Lagrangian form [45]. The JADCE is solved via AEM-ADMM by updating the set of variables $\{\mathbf{X}_g,\mathbf{Z}_g,\boldsymbol{\Theta}_g\}$ in an alternating manner. Precisely, the sub-problems corresponding to the variables are each given in the $(t+1)$-th iteration by

$$\begin{aligned}\mathbf{Z}_g^{(t+1)} &= \min_{\mathbf{Z}_g}\mathcal{L}\left(\mathbf{X}_g^{(t)},\mathbf{Z}_g,\boldsymbol{\Theta}_g^{(t)}\right)\\ &= \min_{\mathbf{Z}_g}\frac{1}{2}\left\|\mathbf{C}_g\left(\mathbf{S}_g\mathbf{Z}_g-\hat{\mathbf{Y}}_g+\boldsymbol{\Psi}_g\right)\right\|_F^2+\left\|\mathbf{X}_g^{(t)}-\mathbf{Z}_g+\frac{\boldsymbol{\Theta}_g^{(t)}}{\rho}\right\|_F^2,\end{aligned} \tag{23}$$

$$\begin{aligned}\mathbf{X}_g^{(t+1)} &= \min_{\mathbf{X}_g}\mathcal{L}\left(\mathbf{X}_g,\mathbf{Z}_g^{(t+1)},\boldsymbol{\Theta}_g^{(t)}\right)\\ &= \min_{\mathbf{X}_g}\left\|\mathbf{X}_g\right\|_{2,1}+\frac{\rho}{2}\|\mathbf{X}_g-\mathbf{Z}_g^{(t+1)}+\frac{1}{\rho}\boldsymbol{\Theta}_g^{(t)}\|_{\mathrm{F}}^2,\end{aligned} \tag{24}$$

$$\boldsymbol{\Theta}_g^{(t+1)} = \boldsymbol{\Theta}_g^{(t)}+\rho\big(\mathbf{X}_g^{(t+1)}-\mathbf{Z}_g^{(t+1)}\big), \tag{25}$$

such that $\mathbf{Z}_g^{(t+1)}$ is updated by minimizing (23) with respect to $\mathbf{Z}_g$ while holding all the other variables constant. That is, computing the derivative with respect to $\mathbf{Z}_g$, setting it to zero and solving for $\mathbf{Z}_g$ as follows

$$\frac{\partial\mathcal{L}\left(\mathbf{X}_g^{(t)},\mathbf{Z}_g,\boldsymbol{\Theta}_g^{(t)}\right)}{\partial\mathbf{Z}_g}=\mathbf{S}_g^{\mathrm{H}}\mathbf{C}_g^{\mathrm{H}}\mathbf{C}_g\mathbf{Z}_g+\rho\mathbf{Z}-\rho\mathbf{X}_g^{(t)}+\boldsymbol{\Theta}_g^{(t)}-\mathbf{S}_g^{\mathrm{H}}\mathbf{C}_g^{\mathrm{H}}\mathbf{C}_g\hat{\mathbf{Y}}_g+\mathbf{S}_g^{\mathrm{H}}\mathbf{C}_g^{\mathrm{H}}\mathbf{C}_g\boldsymbol{\Psi}_g=\mathbf{0}, \tag{26}$$

which leads to

$$\mathbf{Z}_g^{(t+1)}=\left(\mathbf{S}_g^{\mathrm{H}}\mathbf{C}_g^{\mathrm{H}}\mathbf{C}_g\mathbf{S}_g+\rho\mathbf{I}_{N_g}\right)^{-1}\left(\rho\mathbf{X}^{(t)}-\boldsymbol{\Theta}_g^{(t)}+\mathbf{S}_g^{\mathrm{H}}\mathbf{C}_g^{\mathrm{H}}\mathbf{C}_g\hat{\mathbf{Y}}_g-\mathbf{S}_g^{\mathrm{H}}\mathbf{C}_g^{\mathrm{H}}\mathbf{C}_g\boldsymbol{\Psi}_g\right). \tag{27}$$

Similarly, the computation of $\mathbf{X}_g^{(t+1)}$ involves minimizing (24) with respect to $\mathbf{X}_g$. By observing that (24) is the Moreau envelope of the mixed norm $\left\|\mathbf{X}_g\right\|_{2,1}$, we can update $\mathbf{X}_g$ based on the results obtained from (27). Therefore, in order to enforce the sparsity of the solution to JADCE, the ℓ_2 norms of the rows of $\mathbf{X}_g$ must be sparse. We can denote the norms of the rows of $\mathbf{X}_g$ by $\bar{\mathbf{x}}_g\in\mathbb{R}^{N_g\times 1}$. Therefore, we update $\mathbf{X}_g$ by solving the following

$$\mathbf{X}_g^{(t+1)}=\min_{\mathbf{X}_g}\left\|\bar{\mathbf{x}}_g\right\|_1+\frac{\rho}{2}\left\|\mathbf{X}_g-\boldsymbol{\Pi}_g^{(t+1)}\right\|_F^2, \tag{28}$$

```
Algorithm 2: AEM-ADMM, $\forall g \in \mathcal{G}$
    Input: $\hat{\mathbf{Y}}_g$, $\Delta$, $\mathbf{C}_g$, $\mathbf{\Psi}_g$
    Initialisation: $\mathbf{X}_g^{(0)} = \mathbf{0}$, $\mathbf{Z}_g^{(0)} = \mathbf{0}$, $\mathbf{\Theta}_g^{(0)} = \mathbf{0}$, $t = 0$
    repeat
        Update $\mathbf{Z}_g^{(t+1)}$ using (27)
        Update $\mathbf{X}_g^{(t+1)}$ using (29)
        $\mathbf{\Theta}_g^{(t+1)} = \mathbf{\Theta}_g^{(t)} + \rho\left(\mathbf{X}_g^{(t+1)} - \mathbf{Z}_g^{(t+1)}\right)$
        $t = t + 1$
    until $\frac{\left\|\mathbf{Z}_g^{(t+1)} - \mathbf{Z}_g^{(t)}\right\|_F}{\left\|\mathbf{Z}_g^{(t)}\right\|_F} < \Delta$;
    Output: $\hat{\mathbf{X}}_g = \mathbf{Z}_g$
```

where $\mathbf{\Pi}_g^{(t+1)} = \mathbf{Z}_g^{(t+1)} + \frac{1}{\rho}\mathbf{\Theta}_g^{(t)}$, and using the proximal operator method [45], one obtains N_g decoupled solutions [50]

$$\mathbf{x}_{n,g}^{(t+1)} = \text{prox}_{\lambda,\|\bar{\mathbf{x}}_g\|_1}(\mathbf{\Pi}_g^{(t+1)}, \rho) = \boldsymbol{\pi}_{n,g}^{(t+1)} \frac{\max\{\|\boldsymbol{\pi}_{n,g}^{(t+1)}\| - \rho^{-1}, 0\}}{\|\boldsymbol{\pi}_{n,g}^{(t+1)}\|}, n = 1, \cdots, N_g. \tag{29}$$

A summary of AEM-ADMM is presented in Algorithm 2. Note that the AEM-ADMM inherits the properties of classical ADMM [45] and thus has slow convergence to the best possible accuracy, even though, most of its results are acceptable for the JADCE framework. Next, we present the AEM-SBL which is the Bayesian solution and thus exploits the statistical distributions of the observations and the prior.

C. Solution via AEM-SBL

The AEM-ADMM developed in Section IV-B relies on a sparsity promoting penalty and not on the explicit prior distribution $\mathcal{P}(\mathbf{X}_g)$, which may be highly sub-optimal. Therefore, we introduce the AEM-SBL, another AEM-inspired JADCE solution that relies on the SBL framework [21], [51]. Given its Bayesian nature, AEM-SBL exploits $\mathcal{P}(\mathbf{X}_g)$, which is a clear advantage over AEM-ADMM. The AEM-SBL uses the joint posterior distribution

$$\begin{aligned}\mathcal{P}(\mathbf{X}_g, \mathbf{\Gamma}_g | \mathbf{Y}_g) &= \frac{\mathcal{P}(\mathbf{Y}_g|\mathbf{X}_g, \mathbf{\Gamma}_g)\mathcal{P}(\mathbf{X}_g|\mathbf{\Gamma}_g)\mathcal{P}(\mathbf{\Gamma}_g)}{\mathcal{P}(\mathbf{Y}_g)} \\ &= \frac{\mathcal{P}(\hat{\mathbf{Y}}_g + \mathbf{\Psi}_g|\mathbf{X}_g, \mathbf{\Gamma}_g)\mathcal{P}(\mathbf{X}_g|\mathbf{\Gamma}_g)\mathcal{P}(\mathbf{\Gamma}_g)}{\mathcal{P}(\mathbf{Y}_g)}, \forall g,\end{aligned} \tag{30}$$

where the second line follows from the corrected likelihood (19), for which $\mathcal{P}(\boldsymbol{y}_m|\mathbf{x}_m) \approx \mathcal{CN}(\mathbf{S}_m\mathbf{x}_m, \mathbf{\Phi}_g)$ as a result of AEM, while $\mathbf{\Gamma}_g = \text{diag}\{\boldsymbol{\gamma}_g\}$, where $\boldsymbol{\gamma}_g = \{\gamma_{1,g}, \cdots, \gamma_{N_g,g}\} \in$

$\mathbb{R}_{+}^{N_g\times 1}$ are the sparsity promoting hyper-parameters in each cluster. Notice that the diagonal precision matrix $\mathbf{\Gamma}_g$ of these hyper-parameters creates a fixed sparsity pattern across each row of $\hat{\mathbf{X}}_g$, and thus allowing the decomposition of the joint posterior distribution in each cluster as follows

$$\mathcal{P}(\mathbf{X}_g,\mathbf{\Gamma}_g|\mathbf{Y}_g)\propto\prod_{m=1}^{M}\mathcal{P}\left(\hat{\mathbf{y}}_m+\boldsymbol{\psi}_m|\mathbf{S}_g\mathbf{x}_m\right)\prod_{n=1}^{N_g}\mathcal{P}\left(\mathbf{x}_{n,g}|\gamma_{n,g}\right)\times\prod_{n=1}^{N_g}\mathcal{P}\left(\gamma_{n,g}\right), \tag{31}$$

allowing independent update of $\gamma_{n,g}$ and $\mathbf{x}_{n,g}$ as will be shown later.

Following the conventional SBL framework, the AEM-SBL uses (31) to find $\boldsymbol{\gamma}_g$ and $\mathbf{X}_g$ using AEM corrected expectation (E) step and the maximization (M)-step, respectively [51], [52]. To facilitate this, we define the AEM-SBL cost as a function of $\boldsymbol{\gamma}_g$ at each cluster, i.e.,

$$\begin{aligned}\boldsymbol{\gamma}_g &= \underset{\boldsymbol{\gamma}_g}{\operatorname{argmax}}\ \ln\mathcal{P}(\boldsymbol{\gamma}_g|\hat{\mathbf{Y}}_g+\mathbf{\Psi}_g)\\ &\propto \underset{\boldsymbol{\gamma}_g}{\operatorname{argmax}}\ \ln\mathcal{P}(\mathbf{Y}_g|\boldsymbol{\gamma}_g)\mathcal{P}(\boldsymbol{\gamma}_g).\end{aligned} \tag{32}$$

Note that the problem (32) requires the marginalization of $\mathcal{P}(\mathbf{X}_g,\mathbf{Y}_g,\boldsymbol{\gamma}_g)$ with respect to $\mathbf{X}_g$, which can be solved iteratively using EM. Therefore, in the $(t+1)$-th iteration, the corrected E-step is computed using the log-likelihood of the complete joint distribution with respect to the posterior distribution that is parameterized on the previous estimate of $\boldsymbol{\gamma}_g$, i.e., $\mathcal{P}(\mathbf{x}_m|\mathbf{y}_m,\boldsymbol{\gamma}_g^{(t)})$. Let this expectation be defined at each antenna by

$$\begin{aligned}J(\boldsymbol{\gamma}_g,\hat{\boldsymbol{\gamma}}_g^{(t)}) &= \mathbb{E}_{\mathcal{P}(\mathbf{x}_m|\mathbf{y}_m,\hat{\boldsymbol{\gamma}}_g^{(t)})}\ln\mathcal{P}(\mathbf{x}_m,\mathbf{y}_m|\boldsymbol{\gamma}_g)\\ &= \mathbb{E}_{\mathcal{P}(\mathbf{x}_m|\mathbf{y}_m,\boldsymbol{\gamma}_g^{(t)})}[\ln\mathcal{P}(\mathbf{x}_m|\boldsymbol{\gamma}_g)+\ln\mathcal{P}(\mathbf{y}_m|\mathbf{x}_m)+\ln\mathcal{P}(\boldsymbol{\gamma}_g)],\forall m\in\mathcal{M}.\end{aligned} \tag{33}$$

The decomposition presented in (31) allows expressing the complete expectation as follows

$$J(\boldsymbol{\gamma}_g,\hat{\boldsymbol{\gamma}}_g)\propto\sum_{n=1}^{N_g}\ln\gamma_{n,g}-\mathbb{E}_{\mathcal{P}(\mathbf{x}_g|\mathbf{y}_g,\boldsymbol{\gamma}_g^{(t)})}[||\mathbf{x}_{n,g}||^2], \tag{34}$$

where the posterior distribution $\mathcal{P}(\mathbf{x}_m|\mathbf{y}_m,\hat{\boldsymbol{\gamma}}_g^{(t)})$ of (33) is parameterized in the AEM framework by the corrected mean and covariance, respectively given by

$$\begin{aligned}\hat{\mathbf{x}}_m &= \mathbf{\Sigma}_g\mathbf{S}_g^{\mathrm{H}}\mathbf{\Phi}_g^{-1}\left(\hat{\mathbf{y}}_m+\boldsymbol{\psi}_m\right),\forall m\in\mathcal{M},\\ \mathbf{\Sigma}_g &= \left(\mathbf{S}_g^{\mathrm{H}}\mathbf{\Phi}_g^{-1}\mathbf{S}_g+\mathbf{\Gamma}_g^{(t)}\right)^{-1}.\end{aligned} \tag{35}$$

Note that each diagonal entry of $\mathbf{\Sigma}_g$, which we denote by $\{\nu_{n,g}\}$ is common for all the entries

Algorithm 3: AEM-SBL, $\forall g \in \mathcal{G}$

```
Input: $\hat{\mathbf{Y}}_g$, $\Delta$, $\mathbf{C}_g$
Initialization: $\mathbf{X}^0 = \mathbf{0}$, $\mathbf{X}^0 = \mathbf{0}$, $\mathbf{\Gamma}^{(0)} = \mathbf{1}_{N_g \times 1}$, $t = 0$
repeat
    Update $\mathbf{X}_g^{(t+1)}$ using (35)
    Update $\mathbf{\Gamma}^{(t+1)}$ using (39)
    $t = t + 1$
until $\frac{\left\|\mathbf{X}_g^{(t+1)} - \mathbf{X}_g^{(t)}\right\|_F}{\left\|\mathbf{X}_g^{(t+1)}\right\|_F} < \Delta$;
Output: $\hat{\mathbf{X}}_{\mathbf{g}} = \mathbf{X}_g^{(t)}$
```

of $\mathbf{x}_{n,g}$. Further, the second term of (34) can be simplified by [53]

$$\mathbb{E}_{\mathcal{P}(\mathbf{x}_g|\mathbf{y}_g,\hat{\boldsymbol{\gamma}}_g^{(t)})}[\|\mathbf{x}_{n,g}\|^2] = \mathbb{E}_{\mathcal{P}(\mathbf{x}_g|\mathbf{y}_g,\boldsymbol{\gamma}_g^{(t)})}[\|\mathbf{x}_{n,g}\|]^2 + \mathbb{V}_{\mathcal{P}(\mathbf{x}_g|\mathbf{y}_g,\boldsymbol{\gamma}_g^{(t)})}[\mathbf{x}_{n,g}], \tag{36}$$

thus, for the n-th device in the g-th cluster

$$J(\gamma_{n,g}, \hat{\gamma}_{n,g}) \propto \text{ln}\gamma_{n,g} - \gamma_{n,g}(\|\hat{\mathbf{x}}_{n,g}\|^2 + \nu_{n,g}). \tag{37}$$

In the M-step, the hyper-parameters are computed for each MTD by solving (32) as follows

$$\frac{\partial J\left(\gamma_{n,g}, \gamma_{n,g}^{(t)}\right)}{\partial \gamma_{n,g}} = \frac{1}{\gamma_{n,g}} - (\|\hat{\mathbf{x}}_{n,g}\|^2 + \nu_{n,g}) = 0, \tag{38}$$

which leads to

$$\gamma_{n,g}^{(t+1)} = \frac{1}{\|\hat{\mathbf{x}}_{n,g}\|^2 + \nu_{n,g}}, \qquad \forall g, n. \tag{39}$$

A summary of the AEM-SBL is given by Algorithm 3.

D. Complexity Analysis

The computational complexity of the algorithms is given in Table I in terms of the big-$\mathcal{O}$ notation, which considers relevant mathematical operations, e.g., matrix multiplications and inversions. All in all, notice that given $N_g < N$, the AEM-ADMM, and the AEM-SBL have reduced computational complexity compared with their conventional implementations. To this end, the proposed cluster-wise AEM algorithms are bound to have shorter runtime as will be seen in the figures.

TABLE I: Computational complexity of different JADCE algorithms

Algorithm	Number of complex operations in each iteration	Computational Complexity
ADMM	$N^2M + NM^2 + MLN$	$\mathcal{O}(N^2M + NM^2)$
AEM-ADMM	$\frac{N^2M}{G^2} + \frac{NM^2}{G} + MLN$	$\mathcal{O}(\frac{N^2M}{G^2} + \frac{NM^2}{G})$
SBL	$N^2L + N^2$ + NM	$\mathcal{O}(N^2L)$
AEM-SBL	$\frac{N^2L}{G} + \frac{N^2}{G}$ + NM	$\mathcal{O}(\frac{N^2L}{G})$
SOMP	$(2L+1)MN + LM^2 + (M+1)L$	$\mathcal{O}(LMN)$
CB-SOMP	$(2L+1)MN + LM^2 + (M+1)L$	$\mathcal{O}(LMN)$

V. NUMERICAL RESULTS AND DISCUSSIONS

In this section, we present the results of the proposed AEM-ADMM and the AEM-SBL in comparison to other JADCE approaches. The numerical results are presented in terms of the channel estimation accuracy, detection capabilities, and scalability via the normalized mean squared error (NMSE), the average probability of miss detection (PMD), and the algorithm run-time, respectively. To clarify, we will only present the performance metrics for cluster-wise performance as they can be easily extended to evaluate the performance of centralized algorithms such as ADMM, SOMP, and SBL.

The channel estimation accuracy is evaluated using the NMSE defined by

$$\text{NMSE}_i = \mathbb{E}_{i,g}\left(\frac{\|\mathbf{x}_{i,g} - \hat{\mathbf{x}}_{i,g}\|^2}{\|\mathbf{x}_{i,g}\|^2}\right), i \in \mathcal{K}_g. \tag{40}$$

For PMD, we first estimate the activity vector $\hat{\boldsymbol{\alpha}}_g \in \{0,1\}^{N_g \times 1}$ using

$$\hat{\alpha}_{n,g} = \begin{cases} 1, & \text{if } \|\hat{\mathbf{x}}_{n,g}\|_2 \geq \zeta \\ 0, & \text{otherwise} \end{cases}, \tag{41}$$

where ζ is a threshold that is set according to a fixed target probability of false alarm (PFA) (see Table II). It then follows that the PMD is computed using

$$\text{PMD} = \mathbb{E}\left(\frac{\sum_{n=1}^{N_g} \max(0, \alpha_{n,g} - \hat{\alpha}_{n,g})}{|\mathcal{K}_g|}\right). \tag{42}$$

The run-time performance is evaluated in seconds, thus related to the number of iterations and the computational complexity analysis that was presented in Table I.

A. Simulation Setup

We consider a massive MIMO uplink scenario, where $N = 1000$ MTDs are divided into $G = 4$ clusters. For simplicity, we adopt a log-distance path loss model and a complex Hadamard

TABLE II: Simulation parameters

Parameter	**Value**
Path loss for distance (km)	$130+37.6\log_{10}(d_{n,g})$ dB
Bandwidth	20 MHz
Noise power (σ^2)	2×10^{-13} W
Coherence interval (T)	300
Cell radius	250 m
Number of MTDs (N)	1000
Number of clusters(G)	4
Length of the pilot sequences (L)	64
Number of BS antennas (M)	32
Activation probability (ϵ)	0.01
Average SNR	10 dB
Error tolerance (Δ)	10^{-4}
Target PFA	10^{-3}

matrix for the basis matrix $\mathbf{B}$ of the pilot sequences. Unless otherwise stated, the simulations are performed using the parameters provided in Table II. The figures display results that were obtained by averaging over 10^3 Monte Carlo simulations.

B. On the length of the pilot sequences

In Fig. 2, we assess the impact of the pilot lengths on the performance of the JADCE algorithms. Specifically, Fig. 2(a) illustrates how the NMSE varies with the under-sampling ratio, which measures the ratio of the pilot length to the number of devices in the network, i.e., $\frac{L}{N}$. In general, the results show that the channel estimation improves with the pilot length-to-device ratio. This is primarily because higher values of $\frac{L}{N}$ enable the BS to allocate more resources during the training phase, thereby improving the accuracy of the CSI. In addition, a higher $\frac{L}{N}$ ratio results in longer pilot sequences, which can promote orthogonality between the pilot sequences of different MTDs, leading to fewer pilot collisions in the network and a higher quality of the channel estimate. Accordingly, as $\frac{L}{N}$ increases, the JADCE algorithms benefit from improved RIP of the matrix $\mathbf{S}_g$. It is noteworthy that both AEM-SBL and AEM-ADMM exhibit similar performance to ADMM and SBL, while solving smaller-sized problems. Therefore, both AEM-ADMM and AEM-SBL are highly efficient methods for performing channel estimation under practical conditions in mMTC, particularly when the pilot length is much smaller than the number of devices in the network, i.e., with $L \ll N$. From the same results, CB-SOMP (Algorithm 1) exhibits poorer channel estimation capabilities than the classical SOMP. This

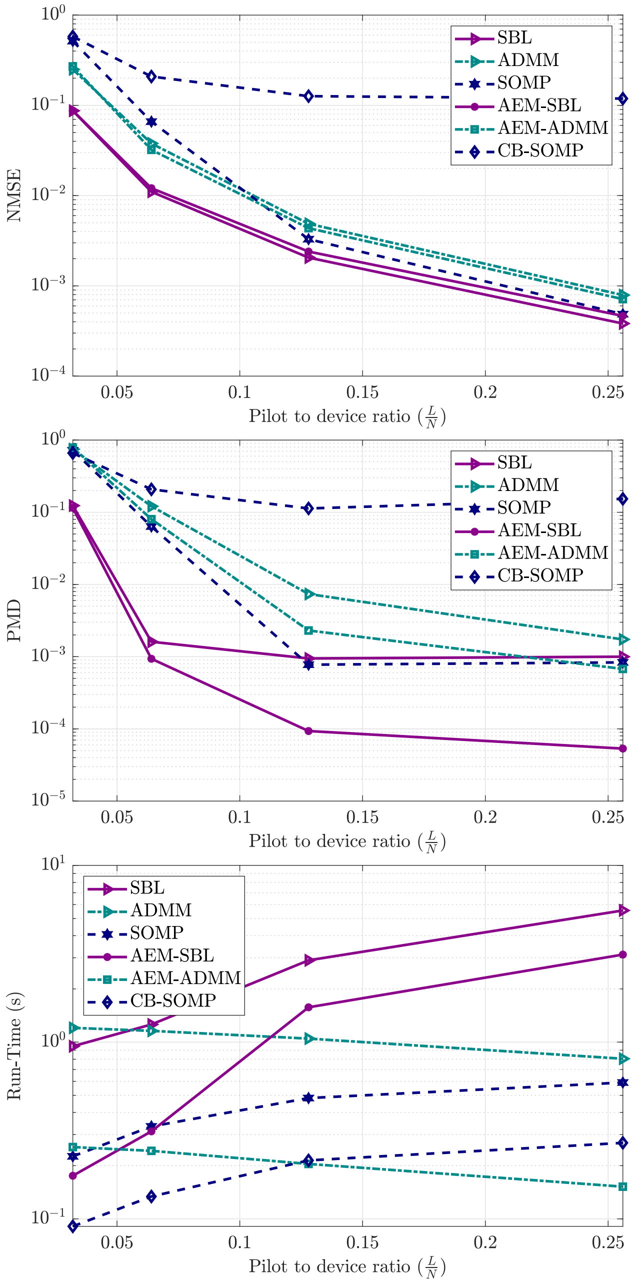

Fig. 2: Performance in terms of a) NMSE (top), b) PMD (middle), and c) run-time (bottom) as a function of the pilot length.

under-performance of CB-SOMP can be attributed to its reliance on a completely mismatched model, thereby highlighting the importance of accounting for such mismatches, as demonstrated by our AEM-inspired algorithms (AEM-ADMM and AEM-SBL). Conversely, while SOMP and ADMM do not leverage the clustering structure, they exhibit strong performance under larger pilot lengths, which is impractical for mMTC applications.

Fig. 2(b) shows how the PMD is affected by $\frac{L}{N}$. In general, the PMD decreases with the pilot-to-device ratio. In connection with the results of Fig. 2(a), this is due to the reduced pilot collisions of the different MTDs. Remarkably, the AEM-SBL outperforms the conventional SBL under this metric as it benefits from reduced inter cluster MUI, making it efficient in imposing the row sparsity in the recovery of the matrix $\mathbf{X}_g$. Furthermore, AEM-ADMM outperforms ADMM in terms of this metric by efficiently handling the MUI, thereby providing a low-complexity alternative JADCE solution for clustered mMTC. To substantiate this, we analyze the runtime as a function of L in Fig. 2(c). From this figure, it is evident that AEM-ADMM and AEM-SBL are more scalable than their classical counterparts. For example, the AEM-SBL runs five times faster than the SBL as L increases. Although Table I indicates that both AEM-ADMM and ADMM's runtimes are insensitive to L, it is worth mentioning that the former exhibits nearly 10 times faster runtime than the latter as L increases, attributed to its faster convergence. Despite its faster runtime compared to SOMP, CB-SOMP generally produces poor results, as demonstrated in Figure 2(a) and 2(b).

C. *On the average SNR*

In Fig. 3, we present the results of the performance as a function of the average SNR. Specifically, Fig. 3(a) illustrates the performance in terms of the NMSE. As shown, the performance of all the JADCE algorithms improves as the signal power gets higher than the noise power, i.e., increasing average SNR. In spite of this, CB-SOMP doesn't improve in performance due to its reliance on the mismatched model. In view of this, increasing SNR increases the amount of the mismatch, thus resulting in inferior performance than other algorithms. For both AEM-SBL and AEM-ADMM, the AEM tends to correct the mismatch more accurately with increased power levels and this results in their superior performance at high SNR. On the other hand, Fig 3(b) shows the performance of AEM-SBL and AEM-ADMM in terms of the PMD. Both of the algorithms generally show improved detection capabilities, i.e., low PMD as the SNR increases. The AEM-SBL remarkably outperforms the AEM-ADMM mainly due to its ability to exploit the information about the distribution of the parameters as discussed in Section IV-C and IV-B.

D. *On the number of antennas in the BS*

In Fig 4, we present the results of the performance as a function of the number of antennas in the BS. For example, the overall trend of Fig. 4(a) shows that all the algorithms improve the

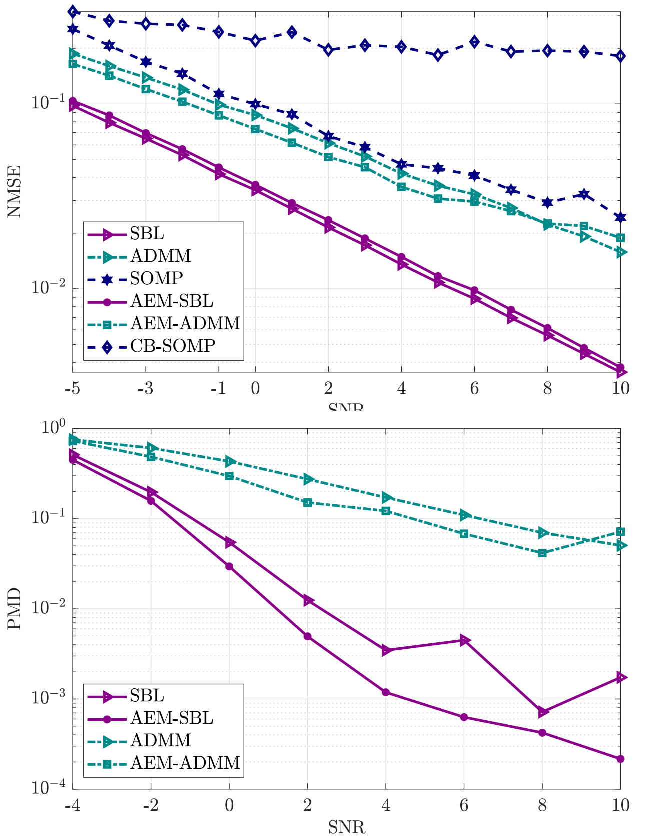

Fig. 3: Performance in terms of a) NMSE (top), b) PMD (bottom) as a function of the SNR.

channel estimation accuracy as the number of antennas at the BS increases. This is mainly due to the fact that the increase in M provides additional structure that can be exploited during the signal recovery process [10], [41]. However, the improvements get to saturation as shown by no substantial improvement beyond $M = 20$, which is consistent with the results of [10]. We also note that both the AEM-SBL and SBL outperform the other algorithms due to their Bayesian nature. Similarly, in Fig. 4(b), the performance in terms of the PMD show an improvement as the number of antenna increases and this is due to the high resolution of the MMV problem under a large number of antennas [54]. However, it is important to note that increasing M has a substantial impact on the run-time and scalability of the algorithms as illustrated in Fig. 4(c), where it is shown that the run-time significantly increases with the number of antennas. This is due to the increasing matrix dimensions. In spite of this, it is evident that both AEM-SBL and AEM-ADMM run faster than their conventional counterparts, thus they may facilitate network scalability. This is one of the major benefits of the proposed algorithms, which exploit the structure of the sensing matrix.

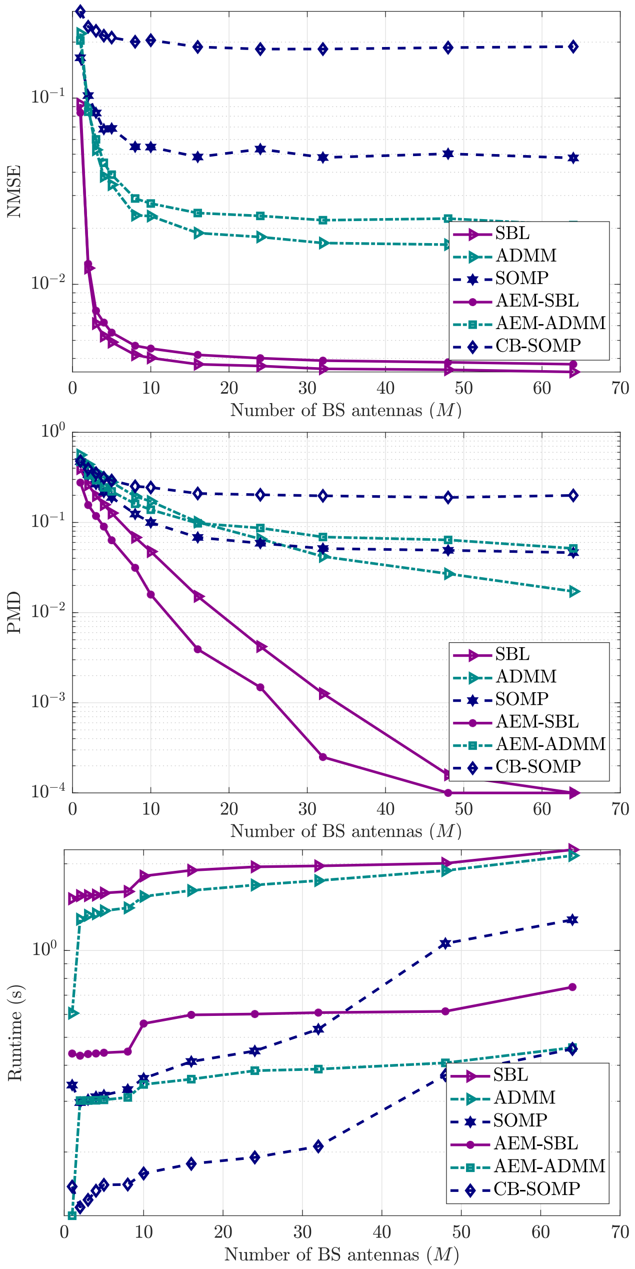

Fig. 4: Performance in terms of a) NMSE (top), b) PMD (middle), and c) run-time (bottom) as a function of the number of antennas.

E. On the activation probability

In Fig. 5, we analyze the impact of the activation probability on the JADCE performance of the algorithms by evaluating NMSE. From the results, it can be observed that all the algorithms perform poorly with decreasing sparsity level, i.e., as more devices are activated at the same time (high ϵ). This is due to the fact that there is an increase in MUI in each cluster when the

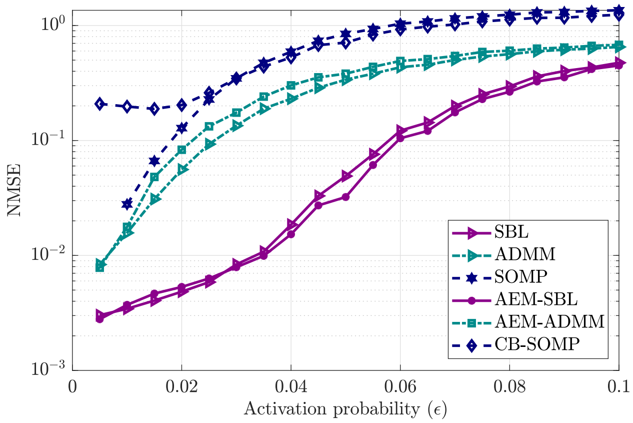

Fig. 5: NMSE as a function of ϵ.

sparsity is decreased. Notably, the AEM-based algorithms demonstrate comparable efficiency to their counterparts by efficiently reducing the MUI, while handling JADCE problems of reduced dimensions.

VI. Conclusion and future works

This work presented a novel framework for cluster-based device activity detection and channel estimation that relies on orthogonal pilot subspaces to optimize GF-NOMA. By utilizing non-i.d.d. pilot sequences, the proposed pilot-based clustering approach promotes efficient device activity detection and enhances network flexibility and scalability, making it practically relevant. We leveraged concepts from the field of inverse problems, and we proposed novel data-driven JADCE solutions: i) AEM-ADMM, which uses iterative soft thresholding for scenarios without exact priors, and ii) AEM-SBL, designed for cases where prior distributions can be formulated. The proposed algorithms offer an advantage over their classical counterparts by improving run-time while maintaining similar performance. Furthermore, the AEM introduces a fresh perspective on device active detection in MTC by accounting for the impairments of sensing matrices. All in all, this work presented a timely solution for receivers in a 5GB cellular network.

As a potential avenue for future research, the AEM approach presented in this work can be further enhanced by introducing adaptive correction parameters at each iteration, which may improve its performance. Additionally, the flat fading channel assumption can be relaxed to frequency selective fading to address orthogonal frequency-division multiplexing (OFDM)-inspired mMTC. Furthermore, the results of this work can be extended to cell-free MIMO communication systems.

References

[1] J. A. Zhang *et al.*, "An overview of signal processing techniques for joint communication and radar sensing," *IEEE Journal of Selected Topics in Signal Processing*, 2021.

[2] M. Renfors, M. Juntti, and M. Valkama, "Signal processing for wireless transceivers," in *Handbook of Signal Processing Systems*. Springer, 2019, pp. 251–310.

[3] M. A. Albreem, M. Juntti, and S. Shahabuddin, "Massive MIMO detection techniques: A survey," *IEEE Communications Surveys & Tutorials*, vol. 21, no. 4, pp. 3109–3132, 2019.

[4] Q. H. Spencer *et al.*, "An introduction to the multi-user MIMO downlink," *IEEE communications Magazine*, vol. 42, no. 10, pp. 60–67, 2004.

[5] R. W. Heath *et al.*, "An overview of signal processing techniques for millimeter wave MIMO systems," *IEEE journal of selected topics in signal processing*, vol. 10, no. 3, pp. 436–453, 2016.

[6] O. López *et al.*, "Statistical Tools and Methodologies for URLLC–A Tutorial," *arXiv preprint arXiv:2212.03292*, 2022.

[7] H. Djelouat *et al.*, "User Activity Detection and Channel Estimation of Spatially Correlated Channels via AMP in Massive MTC," in *2021 55th Asilomar Conference on Signals, Systems, and Computers*. IEEE, 2021, pp. 1200–1204.

[8] L. Marata *et al.*, "Joint channel estimation and device activity detection in heterogeneous networks," in *29th European Signal Processing Conference (EUSIPCO)*. IEEE, 2021, pp. 836–840.

[9] M. B. Shahab *et al.*, "Grant-free non-orthogonal multiple access for IoT: A survey," *IEEE Communications Surveys & Tutorials*, vol. 22, no. 3, pp. 1805–1838, 2020.

[10] K. Senel and E. G. Larsson, "Grant-free massive MTC-enabled massive MIMO: A compressive sensing approach," *IEEE Transactions on Communications*, vol. 66, no. 12, pp. 6164–6175, 2018.

[11] T. Li *et al.*, "Joint Device Detection, Channel Estimation, and Data Decoding with Collision Resolution for MIMO Massive Unsourced Random Access," *IEEE Journal on Selected Areas in Communications*, vol. 40, no. 5, pp. 1535–1555, 2022.

[12] A. Fengler *et al.*, "Non-bayesian activity detection, large-scale fading coefficient estimation, and unsourced random access with a massive MIMO receiver," *IEEE Transactions on Information Theory*, vol. 67, no. 5, pp. 2925–2951, 2021.

[13] X. Shao *et al.*, "Cooperative activity detection: Sourced and unsourced massive random access paradigms," *IEEE Transactions on Signal Processing*, vol. 68, pp. 6578–6593, 2020.

[14] B. Li, J. Zheng, and Y. Gao, "Compressed sensing based multiuser detection of grant-free NOMA with dynamic user activity," *IEEE Communications Letters*, vol. 26, no. 1, pp. 143–147, 2021.

[15] L. Liu *et al.*, "Sparse signal processing for grant-free massive connectivity: A future paradigm for random access protocols in the Internet of Things," *IEEE Signal Processing Magazine*, vol. 35, no. 5, pp. 88–99, 2018.

[16] R. B. Di Renna *et al.*, "Detection techniques for massive machine-type communications: Challenges and solutions," *IEEE Access*, vol. 8, pp. 180 928–180 954, 2020.

[17] Y. Zhu *et al.*, "OFDM-based massive grant-free transmission over frequency-selective fading channels," *IEEE Transactions on Communications*, 2022.

[18] W. Jiang, Y. Jia, and Y. Cui, "Statistical device activity detection for OFDM-based massive grant-free access," *IEEE Transactions on Wireless Communications*, 2022.

[19] O. L. López *et al.*, "Ultra-low latency, low energy, and massiveness in the 6G era via efficient CSIT-limited scheme," *IEEE Communications Magazine*, vol. 58, no. 11, pp. 56–61, 2020.

[20] H. Q. Ngo *et al.*, "Cell-free massive MIMO: Uniformly great service for everyone," in *IEEE 16th international workshop on signal processing advances in wireless communications (SPAWC)*. IEEE, 2015, pp. 201–205.

[21] A. Rajoriya, S. Rukhsana, and R. Budhiraja, "Centralized and decentralized active user detection and channel estimation in mMTC ," *IEEE Transactions on Communications*, vol. 70, no. 3, pp. 1759–1776, 2022.

[22] U. K. Ganesan, E. Björnson, and E. G. Larsson, "Clustering-based activity detection algorithms for grant-free random access in cell-free massive MIMO," *IEEE Transactions on Communications*, vol. 69, no. 11, pp. 7520–7530, 2021.

[23] S. Kim, J. Choi, and J. Park, "Downlink NOMA for short-packet Internet-of-Things communications with low-resolution ADCs," *IEEE Internet of Things Journal*, 2022.

[24] Y. Abdi and T. Ristaniemi, "Optimization of linearized belief propagation for distributed detection," *IEEE Transactions on Communications*, vol. 68, no. 2, pp. 959–973, 2019.

[25] S. Liu, H. Zhang, and Q. Zou, "Decentralized channel estimation for the uplink of grant-free massive machine-type communications," *IEEE Transactions on Communications*, vol. 70, no. 2, pp. 967–979, 2021.

[26] S. Elhoushy, M. Ibrahim, and W. Hamouda, "Cell-free massive MIMO: A survey," *IEEE Communications Surveys & Tutorials*, vol. 24, no. 1, pp. 492–523, 2021.

[27] H. He *et al.*, "Distributed expectation propagation detection for cell-free massive MIMO," in *IEEE Global Communications Conference (GLOBECOM)*. IEEE, 2021, pp. 01–06.

[28] J. Li *et al.*, "Covariance-based activity detection with orthogonal pilot sequences for cell-free distributed massive MIMO systems," *IEEE Transactions on Vehicular Technology*, 2022.

[29] J. Bai and E. G. Larsson, "Activity detection in distributed MIMO: Distributed AMP via likelihood ratio fusion," *IEEE Wireless Communications Letters*, vol. 11, no. 10, pp. 2200–2204, 2022.

[30] Y. Li *et al.*, "Asynchronous activity detection for cell-free massive MIMO: From centralized to distributed algorithms," *IEEE Transactions on Wireless Communications*, 2022.

[31] S. Chen *et al.*, "Structured massive access for scalable cell-free massive MIMO systems," *IEEE Journal on Selected Areas in Communications*, vol. 39, no. 4, pp. 1086–1100, 2020.

[32] F. A. De Figueiredo *et al.*, "On the application of massive MIMO systems to machine type communications," *IEEE Access*, vol. 7, pp. 2589–2611, 2018.

[33] H. Iimori *et al.*, "Joint activity and channel estimation for extra-large MIMO systems," *IEEE Transactions on Wireless Communications*, 2022.

[34] L. Marata *et al.*, "Joint coherent and non-coherent detection and decoding techniques for heterogeneous networks," *IEEE Transactions on Wireless Communications*, 2022.

[35] M. Mozumder *et al.*, "A model-based iterative learning approach for diffuse optical tomography," *IEEE Transactions on Medical Imaging*, vol. 41, no. 5, pp. 1289–1299, 2021.

[36] S. Lunz *et al.*, "On learned operator correction in inverse problems," *SIAM Journal on Imaging Sciences*, vol. 14, no. 1, pp. 92–127, 2021.

[37] J. Kaipio and E. Somersalo, *Statistical and computational inverse problems*. Springer Science & Business Media, 2006, vol. 160.

[38] J. Zhang *et al.*, "Physics-inspired compressive sensing: Beyond deep unrolling," *IEEE Signal Processing Magazine*, vol. 40, no. 1, pp. 58–72, 2023.

[39] Y. C. Eldar and G. Kutyniok, *Compressed sensing: theory and applications*. Cambridge university press, 2012.

[40] Z. Chen, F. Sohrabi, and W. Yu, "Sparse activity detection for massive connectivity," *IEEE Transactions on Signal Processing*, vol. 66, no. 7, pp. 1890–1904, 2018.

[41] Z. Wei, D. W. K. Ng, and J. Yuan, "Joint pilot and payload power control for uplink MIMO-NOMA with MRC-SIC receivers," *IEEE Communications Letters*, vol. 22, no. 4, pp. 692–695, 2018.

[42] R. B. Di Renna and R. C. de Lamare, “Joint channel estimation, activity detection and data decoding based on dynamic message-scheduling strategies for mMTC,” *IEEE Transactions on Communications*, vol. 70, no. 4, pp. 2464–2479, 2022.

[43] L. Liu *et al.*, “A new insight into GAMP and AMP,” *IEEE Transactions on Vehicular Technology*, vol. 68, no. 8, pp. 8264–8269, 2019.

[44] D. Zhang *et al.*, “Unifying message passing algorithms under the framework of constrained bethe free energy minimization,” *IEEE Transactions on Wireless Communications*, vol. 20, no. 7, pp. 4144–4158, 2021.

[45] S. Boyd, N. Parikh, and E. Chu, *Distributed optimization and statistical learning via the alternating direction method of multipliers*. Now Publishers Inc, 2011 .

[46] H. Djelouat, M. Leinonen, and M. Juntti, “Spatial correlation aware compressed sensing for user activity detection and channel estimation in massive MTC,” *IEEE Transactions on Wireless Communications*, 2022.

[47] T. T. Cai and L. Wang, “Orthogonal matching pursuit for sparse signal recovery with noise,” *IEEE Transactions on Information theory*, vol. 57, no. 7, pp. 4680–4688, 2011.

[48] S. Arridge *et al.*, “Approximation errors and model reduction with an application in optical diffusion tomography,” *Inverse problems*, vol. 22, no. 1, p. 175, 2006.

[49] A. Wiesel, Y. C. Eldar, and A. Yeredor, “Linear regression with gaussian model uncertainty: Algorithms and bounds,” *IEEE Transactions on Signal Processing*, vol. 56, no. 6, pp. 2194–2205, 2008.

[50] T. Goldstein, C. Studer, and R. Baraniuk, “A field guide to forward-backward splitting with a FASTA implementation,” *arXiv preprint arXiv:1411.3406*, 2014.

[51] Z. Zhang and B. D. Rao, “Sparse signal recovery with temporally correlated source vectors using sparse Bayesian learning,” *IEEE Journal of Selected Topics in Signal Processing*, vol. 5, no. 5, pp. 912–926, 2011.

[52] A. Sant, M. Leinonen, and B. D. Rao, “Block-sparse signal recovery via general total variation regularized sparse bayesian learning,” *IEEE Transactions on Signal Processing*, vol. 70, pp. 1056–1071, 2022.

[53] M. Al-Shoukairi, P. Schniter, and B. D. Rao, “A GAMP-based low complexity sparse bayesian learning algorithm,” *IEEE Transactions on Signal Processing*, vol. 66, no. 2, pp. 294–308, 2017.

[54] B. Zheng *et al.*, “Joint sparse recovery for signals of spark-level sparsity and MMV tail-$\ell_{2,1}$ minimization,” *IEEE Signal Processing Letters*, vol. 28, pp. 1130–1134, 2021.